HHS Public Access

Author manuscript

Biotechnol Bioeng. Author manuscript; available in PMC 2021 November 22.

Published in final edited form as:

Biotechnol Bioeng. 2020 June ; 117(6): 1826–1838. doi:10.1002/bit.27308.

Microstructural densification and alignment by aspiration-ejection influence cancer cell interactions with three-dimensional collagen networks

Ruby N. Huynh[1], **Manal Yousof**[1], **Khanh L. Ly**[1], **Farai C. Gombedza**[2], **Xiaolong Luo**[3], **Bidhan C. Bandyopadhyay**[1,2], **Christopher B. Raub**[1]

[1]Department of Biomedical Engineering, The Catholic University of America, Washington, District of Columbia

[2]Research Service, Veterans Affairs Medical Center, Washington, District of Columbia

[3]Department of Mechanical Engineering, The Catholic University of America, Washington, District of Columbia

Abstract

Extracellular matrix microstructure and mechanics are crucial to breast cancer progression and invasion into surrounding tissues. The peritumor collagen network is often dense and aligned, features which in vitro models lack. Aspiration of collagen hydrogels led to densification and alignment of microstructure surrounding embedded cancer cells. Two metastasis-derived breast cancer cell lines, MDA-MB-231 and MCF-7, were cultured in initially 4 mg/ml collagen gels for 3 days after aspiration, as well as in unaspirated control hydrogels. Videomicroscopy during aspiration, and at 0, 1, and 3 days after aspiration, epifluorescence microscopy of phalloidin-stained F-actin cytoskeleton, histological sections, and soluble metabolic byproducts from constructs were collected to characterize effects on the embedded cell morphology, the collagen network microstructure, and proliferation. Breast cancer cells remained viable after aspiration-ejection, proliferating slightly less than in unaspirated gels. Furthermore, MDA-MB-231 cells appear to partially relax the collagen network and lose alignment 3 days after aspiration. Aspiration-ejection generated aligned, compact collagen network microstructure with immediate cell co-orientation and higher cell number density apparently through purely physical means, though cell-collagen contact guidance and network remodeling influence cell organization and collagen network microstructure during subsequent culture. This study establishes a platform to determine the effects of collagen density and alignment on cancer cell behavior, with translational potential for anticancer drug screening in a biomimetic three-dimensional matrix microenvironment, or implantation in preclinical models.

Correspondence Christopher B. Raub, Department of Biomedical Engineering, Catholic University of America, 620 Michigan Ave NE, Pangborn Hall 121, Washington DC 20064. raubc@cua.edu.

CONFLICT OF INTERESTS

The authors declare that there are no conflict of interests.

SUPPORTING INFORMATION

Additional supporting information may be found online in the Supporting Information section.

Keywords

actin cytoskeleton; cancer cells; collagen hydrogel; collagen network microstructure; mechanobiology

1 | INTRODUCTION

The tissue microenvironment plays a critical part in the progression of multiple lethal diseases including cancer (Brabek, Mierke, Rosel, Vesely, & Fabry, 2010). The extracellular matrix (ECM) serves as the scaffolding of the tissue microenvironment and regulates resident cell morphology (Yeung et al., 2005), differentiation (Engler, Sen, Sweeney, & Discher, 2006), migration (Pelham & Wang, 1997), and tissue development to its ultimate functional form (Guo, Frey, Burnham, & Wang, 2006; Reinhart-King, Dembo, & Hammer, 2008; Shebanova & Hammer, 2012). Fibrillar collagen is a predominant component of the ECM in many interstitial tissues that surround tumors and through which cancer cells migrate to form distant metastases. Indeed, collagen microstructural remodeling occurs in the tumor microenvironment and guides tumor cell intravasation (Han et al., 2016). ECM mechanics and ligands independently influence the survival of glioblastoma cells in the presence of toxic compounds (Zustiak et al., 2016). Evidence exists for both inhibition and enhancement of cancer cell proliferation and transport by the surrounding collagen network (Fang, Yuan, Peng, & Li, 2014).

The interstitial collagen network is of critical clinical importance to breast cancer. The relationship between ECM and breast cancer risk is grounded in evidence that patients with denser breast tissue develop a higher than the fourfold increased risk of breast cancer (Boyd et al., 2001). Furthermore, the microstructure of collagen fibers around tumors can be used as an independent hallmark for clinical diagnosis (Conklin et al., 2011). Observations of collagen within and adjacent to tumors have identified certain collagen network microstructures corresponding to disease aggressiveness, known as tumor-associated collagen signatures (TACS; Provenzano et al., 2006). Using nonlinear laser scanning microscopy of the second harmonic signal from collagen, Provenzano et al. (2006) found three TACS that characterize different stages of tumorigenesis. TACS-1 indicates the presence of dense collagen near the tumor region. TACS-2 is characterized by tangentially stretched collagen fibers adjacent to a relatively smooth tumor border that is usually seen in benign cases. TACS-3, found in advanced stages, consists of collagen bundles aligned normal to the tumor boundary displaying an irregular shape. TACS-3 is believed to support malignant cell invasion of the ECM. In addition, the microstructure of collagen is distinct inside tumors compared with juxta- and extratumoral regions (Esbona et al., 2018). Intratumoral collagen fibers were found to be much straighter than in normal interstitium, and are also referred to as TACS-3 (Provenzano et al., 2006). These signatures raise questions about the effects on cancer progression of mechanobiological interactions between cancer cells and aligned, dense collagen networks.

Dense biopolymer matrices typically have higher mechanical stiffness, denser presentation of cell-matrix attachment sites, and smaller pores than sparse biopolymer networks.

Substrate stiffness has been manipulated in synthetic polymer systems, yielding cancer mechanobiological insight. For example, on stiff but not compliant two-dimensional polyacrylamide substrates coated with Type I collagen, hepatocellular carcinoma cells upregulate vascular endothelial growth factor dependent upon β1 integrin signaling (Dong et al., 2014). Demonstrating the importance of the topology and biochemistry of the extracellular microenvironment, protease inhibitors prevent migration in three-dimensional polyethylene glycol hydrogels engineered with proteolytically degradable crosslinks, but not in natural collagen and fibrin gels fibrin with larger and more labile pores (Raeber, Lutolf, & Hubbell, 2005). In contrast to synthetic polymer systems, in native biopolymer hydrogels, strategies have focused on altering mechanical properties through control of microstructure: collagen fiber and pore dimensions (Raub et al., 2007), alignment (Vader, Kabla, Weitz, & Mahadevan, 2009), polymer concentration (Zaman et al., 2006), and exogenously-added crosslinks (Levental et al., 2009). More recently in biopolymer gels, local matrix stiffness has been assessed using active microrheology (Keating, Kurup, Alvarez-Elizondo, Levine, & Botvinick, 2017), revealing steep gradients in the mechanics of pericellular material, which can be actively modulated through targeted and focused laser-induced ruthenium-catalyzed photocrosslinking (Keating, Lim, Hu, & Botvinick, 2019). Assessment and control of microstructural and mechanical properties of collagen gels are important as such properties promote angiogenesis (Bordeleau et al., 2017), enhance persistent migration (Riching et al., 2014) and prime epithelial-to-mesenchymal transition in cancer cells (Wei et al., 2015).

Biofabrication of in vitro collagen scaffolds controls biophysical and microstructural features of the collagen network relevant to embedded cell behavior. Plastic compression generates a more than 100-fold volumetric reduction of collagen hydrogels within a few minutes, creating a platform of dense collagen (Brown, Wiseman, Chuo, Cheema, & Nazhat, 2005) that stimulates osteogenesis (Yuan et al., 2018) and nurtures corneal stem cells (Mi, Chen, Wright, & Connon, 2010), both of which reside in collagen-dense tissues in vivo. Reverse dialysis followed by evaporation is another method to create uniform, dense collagen networks by inducing liquid crystallization (Knight, Nash, Hu, Haffegee, & Ho, 1998), then allowing slow removal of the acidic component in collagen gels (Bessea, Coulomb, Lebreton-Decoster, & Giraud-Guille, 2002). These methods were used to generate in vitro bone scaffolds (Thula et al., 2011). An initially disorganized collagen network microstructure limits the amount of global microstructural remodeling by corneal fibroblasts, highlighting the general need to produce initially biomimetic microstructures in three-dimensional in vitro cultures (Saeidi et al., 2012). Such a need requires a flexible, controllable way to exert compressive, tensile, and shear stresses on ECM hydrogels to control microstructure without destroying embedded cells.

Aspiration-ejection is a recently proposed method to produce aligned, dense collagen constructs (Kamranpour, Miri, James-Bhasin, & Nazhat, 2016; Miri et al., 2016). By this technique, aspiration of a collagen gel adherent on a filter membrane into a narrow-gauge syringe draws the gel into a cylindrical shape, producing higher density from compaction and alignment from elongation during aspiration. The level of compaction depended on needle gauge, from 0.3 to 0.9 mm (Marelli, Ghezzi, James-Bhasin, & Nazhat, 2015). The alteration in the microstructure of the aspirated gel-accelerated osteoblastic differentiation and supported neuronal transdifferentiation of embedded mesenchymal stem

cells (Kamranpour et al., 2016; Marelli et al., 2015). The resulting cell-seeded scaffolds were proposed to be injectable as biologic implants for tissue restoration. It remains to be seen whether this technique can be adapted to produce dense, aligned cancer cell constructs, and subsequent behavior of the cancer cells during postaspiration culture.

Based on previous studies of gel aspiration with noncancer cells, we hypothesized that cancer cells seeded in aspirated collagen gels would sustain mechanical damage but retain viability, allowing subsequent culture in a dense, aligned collagen scaffold. To test this hypothesis, two breast cancer cell lines, MDA-MB-231 and MCF-7, with low and high cell–cell adhesion, respectively, were embedded in aspirated gels designed for individual floating culture, and we determined the effects of aspiration-ejection on (a) collagen network microstructure, (b) cell morphology, and (c) cell proliferation up to 3 days after aspiration, compared with unaspirated control gels. Results confirm immediate alignment of embedded cancer cells with collagen network anisotropy introduced by the aspiration, some relaxation of the collagen network and coaligned cells by 3 days of postaspiration culture, and proliferation of embedded cancer cells when the constructs were formed by a gentle method. These findings are significant toward determining breast cancer cell behavior in aligned, dense collagen microenvironments.

2 | MATERIALS AND METHODS

2.1 | Cell culture

Two breast cancer cell lines MDA-MB-231 and MCF-7, a generous gift from Dr Zaver Bhujwalla (John Hopkins School of Medicine, Baltimore, MD), were cultured in Dulbecco's modified Eagle's media (DMEM) containing 10% fetal bovine serum (FBS) on tissue-culture treated polystyrene dishes (VWR International, Radnor, PA). All cells were maintained in an incubator at 37°C, 5% CO_2, and 100% humidity. The cells were trypsinized when reaching 70% confluency, centrifuged at 200*g* and counted using a hemacytometer before diluting into a collagen solution on the ice at 100,000 cells/ml.

2.2 | Collagen hydrogel preparation

Collagen hydrogels were prepared on ice at concentrations of 4 mg/ml from high concentrated Type I rat tail tendon collagen (Corning, NY), 10X phosphate-buffered saline (PBS; Sigma-Aldrich, St. Louis, MO) with phenol red added at 0.159 mg/ml as a pH indicator, and deionized (DI) water. The mixture was neutralized to pH 7.4 by adding a small amount of 0.1 M sodium hydroxide until the color turned cherry red. Cells were seeded into collagen at 100,000 cells/ml. The final solution was well mixed before transferring 2 ml into a 35 mm-diameter Petri dish (Figure 1a). The gels were self-assembled at room temperature for 45 min. Prewarmed nutrient media (1 ml of DMEM containing 10% FBS) was added on top of the gel in the dish and moved to the incubator for 24 hr. After this period, the cell-seeded collagen gels were subjected to micropipette aspiration-ejection under sterile conditions (Figure 1b,c), then returned to the incubator with fresh media for an additional 24–72 hr of culture, with an additional assessment at 0 hr, immediately after aspiration (Figure 1d).

2.3 | Micropipette aspiration

Micropipette gel aspiration-ejection (GAE), a variant of needle-based GAE, was performed as described below (Figure 1). Free-floating, cylindrical, cell-seeded collagen disks were created from the cell and collagen layer in Petri dishes in two ways: (a) by pressing down and gently rotating a 3-mm diameter dermal punch (Sklar Corporation, West Chester, PA; Figure 1a), or alternatively, using a poly-dimethylsiloxane (PDMS) mold to form the gel constructs and allow them to be gently extruded by a stream of media from a pipette (Figure S2). The collagen disks were transferred directly to a micropipette aspiration set-up (Figure 1b) in a sterile biosafety hood, or by spatula to the stage of an inverted phase-contrast microscope (CK30; Olympus Corporation of the Americas, Center Valley, PA), to record images of the aspiration process. In the latter case, the imaging chamber consisted of a space made by microscope slides above and below 2-mm tall spacers, in which a droplet of PBS was held by surface cohesion to both glass surfaces. The end of a borosilicate glass capillary tube, with inner diameter of 0.8 mm and outer diameter of 1 mm (Cole-Parmer, Vernon Hills, IL) was aligned parallel to the gel floating in the PBS droplet, just visible in the microscope's field of view, and was attached to a pneumatic oil aspirator/injector (IM-6; Narishige International, Amityville, NY). The capillary tube was briefly fired in a Bunsen burner to create smooth edges, rinsed with 70% ethanol and sterile DI water, and dried before use. Images were captured at 11 frames per second during aspiration by a CMOS digital microscope camera (MU300; Amscope, Irvine, CA). Defined aspiration steps were created by marking the syringe control knob at 4.7° intervals (defined as 1 step) and attaching a rigid chamber containing a pressure sensor (BMP 180; Adafruit, New York, NY) to the end of the capillary tube (Figure 1b). A linear calibration of ~100 Pa/step was obtained for 60 × 4.7° steps or 282° of rotation of the control knob. A high-pressure aspiration was defined as a rapid rotation of the control knob 180°, about 38 steps, corresponding to 3.8 kPa of applied pressure. After 30 s in the capillary tube, the gels were ejected back into DMEM culture media in new Petri dishes. Alternatively, a low-pressure aspiration was defined as a pressure step of ~200 Pa every 20 s, until the gel collapsed into the capillary tube while experiencing a gradually built-up aspiration pressure.

Two sets of GAE experiments were performed. In the first experiment, MDA-MB-231 cancer cell-seeded gels were aspirated using high- and low-pressure protocols, and varying capillary tube orientation at 10°, 60°, and 90° with respect to the plane of the collagen gel disk (Figure S3). These gels, $n = 7–10$ per group, were imaged under brightfield microscopy using a ×4 objective, and their projected area and aspect ratio were quantified using measurements from the manual tracing of the gel outline in ImageJ. In the second experiment, gels were cultured seeded with MDA-MB-231 and MCF-7 cells as described above and cultured for 0, 1, and 3 days after aspiration, as well as unaspirated gels (Figure 1d). These gels were created by the dermal punch method and examined by confocal microscopy and histology; or created by the gentler PDMS mold method and evaluated for cell proliferation by 2,3-Bis(2-methoxy-4-nitro-5-sulfophenyl)-2H-tetrazolium-5-carboxanilide salt (XTT) assay (Kit III; PromoCell, Heidelberg, Germany) fixed in 10% neutral-buffered formalin at each timepoint for microscopy and histology. The dermal punch experiment consisted of $n = 8$ gels per timepoint, or 96 constructs in total for (2 cell types [MDA-MB-231, MCF-7] × 2 levels

of aspiration [none, high] × 3 culture time points [0, 1, and 3 days]). The PDMS mold experiment consisted of $n = 5$ gels per condition for the same treatments and time points, for a total $n = 60$ gel constructs.

2.4 | Immunofluorescence and reflectance confocal microscopy

Aspirated and unaspirated cell-seeded collagen gels were fixed in formalin, rinsed, and permeabilized with 0.01% Triton-X before fluorescent staining. Alexa Fluor 568-conjugated phalloidin (Life Technologies, Carlsbad, CA) was used to label the F-actin cytoskeleton of cells in the constructs. Imaging was performed using a Zeiss LSM 710 confocal microscope (Zeiss, Jena, Germany) with an argon laser that delivered 0.12 mW of 561 nm wavelength to the gel-cell constructs. The objective lenses of ×10/0.3 numerical aperture (NA) and ×63/1.4NA were dry and immersion oil-coupled to the sample coverslip, respectively. Scanning in the x–y plane was implemented using a 512 × 512 pixel window equaling 0.26 × 0.26 μm pixel lateral dimensions and 0.69 μm in axial z-step for imaging with the ×63 objective or 1.66 × 1.66 μm and 13.37 μm in z-step for imaging with the ×10 objective. Images were taken using ZEN 2010 software (Zeiss) at 8-bit depth (per pixel) simultaneously collecting a 561 nm reflectance channel with neutral density filter and a fluorescence emission channel with a bandpass filter from 565 to 665 nm. Reflectance signals from the collagen matrix and fluorescent signals of F-actin were acquired simultaneously and coregistered using the ImageJ software (NIH). Confocal micrographs containing coregistered red fluorescence and reflectance channels were stitched together using MosaicJ (Thevenaz & Unser, 2007)

2.5 | Histology

Histological sections were created from formalin-fixed, paraffin-embedded tissue constructs, and stained with hematoxylin and eosin for visualization of cells and ECM (Histoserv, Germantown, MD). Brightfield images were taken of the sections with an Amscope ME300 camera through the ×10/0.25 NA objective of the CK30 inverted microscope and across the sections in overlapping fields of view. Images were stitched together to form mosaics using Photoshop (Adobe Systems, Mountain View, CA). The number of nuclei in each tissue section were counted, and the area of the section, in mm^2, was measured using the polygonal region-of-interest tool in ImageJ (NIH).

2.6 | XTT assay

The XTT assay was performed according to the manual (PromoCell XTT Kit III), in a flat-bottomed 96 well-plate (Corning). A working solution of 10 ml of XTT reagent was mixed with 50 μl of activation reagent immediately upon thawing, and then 50 μl was added to each well containing a tissue construct and 100 μl of freshly changed nutrient media. After a 2 hr incubation period in standard tissue culture conditions (37°C, 5% CO_2, 100% humidity), the well-plate was removed and media transferred to a new well-plate, minus the opaque constructs, for optical readout. Absorbance was read on a standard colorimetric microplate reader with filters at 490 and 650 nm. The absorbances were subtracted, $A_{490\ nm} - A_{650\ nm}$, and also corrected for a blank media well (never exposed to cells) to yield a final absorbance. Absorbance values were normalized to the group average of unaspirated controls containing MDA-MB-231 and MCF-7 cells.

2.7 | Image analysis

Confocal fluorescence images were background-subtracted by thresholding at a consistent level across all images, before additional image processing. The F-actin area fraction was obtained by dividing the number of pixels containing phalloidin stain to the total area of the gel in a single confocal image plane, measured from overlapping confocal reflectance images using the trace tool in ImageJ. Digital image correlation was performed using a previously published method (Eberl, 2020; Jones, Silberstein, White, & Sottos, 2014).

Confocal image overlays were constructed by taking the maximum signal projection of the red channel (cell phalloidin stain) overlaid on a single confocal reflectance frame to clearly resolve the collagen network, or a sum of reflectance frames to capture the morphology of the aspirated gel. Orientation vector fields were overlaid on these frames using OrientationJ (Fonck et al., 2009; Rezakhaniha et al., 2012). Local collagen network anisotropy was assessed as the standard deviation (SD) of the orientation map produced in OrientationJ, for a local window of 20 pixels (5.3 μm in confocal images acquired with a ×63 objective). Coalignment of collagen and cells was assessed from images acquired with a ×10 objective by manually tracing 38 individual cells per group in the ImageJ, extracting the long axis orientation, and calculating the cosine of the difference angle between the two, $\cos(\Delta\theta)$. This quantity is 1 for perfect coalignment, and 0 for perpendicular collagen alignment and cell long axis.

2.8 | Statistical analysis

To assess the effects of aspiration and culture time on two breast cancer cell lines, two-factor analysis of variance (ANOVA) was performed on phalloidin-stained area fraction and cell density, in $\#/mm^2$, measured from histological sections. Following two-factor ANOVA, one-factor ANOVA on significant factors from two-factor analysis and pairwise comparisons were performed, the latter using Tukey's posthoc test for differences between culture times, Dunnett's test to compare to unaspirated controls at Day 0. All ANOVA was performed after testing for normality and equal variance by Kolmogorov–Smirnov and Levene's test, respectively, and inspection of the distribution of residuals. If these tests failed, the nonparametric the Kruskal–Wallis test was performed. To assess the effects of aspiration, culture time, and cell type on proliferation, collagen network anisotropy and cell coalignment with collagen, three-factor ANOVAs were performed. For selected pairwise group comparisons, Student's t tests were also performed. Significance for all tests was set at $p < .05$.

3 | RESULTS

3.1 | Aspiration-ejection creates a dense tissue construct dependent upon applied pressure

Aspiration of the collagen gel disks (Figures 2a and 2d) creates a compact, pill-shaped construct (Figures 2c and 2f). For the low-pressure aspiration, after 24–32 steps, the gel deformed in a delayed process leading to total aspiration into the capillary tube (Figure 2bi-iii). Manual tracking of displacement markers (Video S1) and digital image correlation (Figure 2di-iii) demonstrated that the leading edge of the gel compacted, the side walls

adjacent to the capillary tube experienced shear, and the trailing edge of the gel folded to enter the capillary tube. The gel shape was stable following ejection (Figures 2c and 2f). For low-pressure aspiration, the gel compaction process took 7 s. In contrast, gels aspirated with 3.8 kPa of pressure (high pressure) immediately entered the capillary tube, too fast to record at 30 frames per second. The geometric features of the aspirated gel construct depended upon the aspiration protocol. There was a significant effect of aspiration pressure protocol on the gel aspect ratio ($F = 6.6$, $p = .02$) and circularity ($F = 6.4$, $p < .05$), but not projected area ($F = 1.4$, $p = .25$; Figure S3a-c). In contrast, the effects of capillary tube angle with respect to the disk plane at 10°, 60°, and 90° on construct projected area and aspect ratio were not significant (Figure S3d-f). Specifically, the gel aspect ratio was 4.4 ± 1.0 under high pressure, and 3.3 ± 1.0 under low-pressure aspiration protocols.

3.2 | GAE alters collagen network microstructure and aligns cells

The collagen network became aligned following aspiration-ejection, visible as striations in the reflectance signal aligned with the gel long axis (Figure 3). Transverse striations appeared by 3 days culture, especially with MDA-MB-231 cells, which were also aligned with the gel long axis (Figure 3a). In contrast, MCF-7 cells did not align as clearly as MDA-MB-231 cells due to their clustered morphology (Figure 3b). Higher-resolution confocal images, however, demonstrated both individual MDA-MB-231 cells (Figure 4a) and MCF-7 cell clusters (Figure 4b) aligning with the collagen network (gray signal, yellow orientation vectors) immediately following aspiration, with a partial apparent loss of the dense, anisotropic network after 3 days culture. Compaction and alignment of the collagen network in aspirated, (+) Asp, versus unaspirated, (−) Asp, gels was also apparent from reflectance signal in higher resolution confocal micrographs (Figure 5a,b), characterized by smaller pores and a finer, striated reflectance texture, again lost by Day 3 of postaspiration culture.

Cell alignment with collagen and collagen network anisotropy were evaluated quantitatively and were higher in aspirated than unaspirated gels (Figure 4c,d). The cell-collagen alignment parameter, $\cos(\Delta\theta)$, was affected by aspiration, culture time and cell type ($F = 9–75$, $p < .001$ for each, $n = 6–9$ fields-of-view per group from $N = 3–4$ constructs). Specifically, $\cos(\Delta\theta)$ was higher at Day 0 ($p < .001$) and Day 1 ($p < .01$) than Day 3. Collagen network anisotropy depended on aspiration status ($F = 75$, $p < .001$) and culture time ($F = 8$, $p < .01$). Specifically, aspirated gels had lower local collagen orientation SD (and therefore higher anisotropy). This measure of microstructural anisotropy was higher particularly at 3 days in constructs with embedded MDA-MB-231 cells ($p < .01$ and $p < .001$ versus 0 and 1 day of postaspiration culture, respectively).

3.3 | Aspiration-ejection alters cancer cell morphology and distribution in dermal-punched gel constructs

Cancer cell morphology and distribution were altered in the aspirated collagen constructs created by dermal punch. The area fraction of the F-actin label within gels was altered following aspiration for both cancer cell lines (Figure 6). Specifically, MCF-7 F-actin area fraction became lower over culture time in aspirated gels (Figures 6a and 6c), from 1.60 ± 0.31% to 1.30 ± 0.24 and 0.36 ± 0.14 at 0, 1, and 3 days after aspiration. Unaspirated gels

had a lower F-actin area fraction initially (0.92 ± 0.30%) but became similar to aspirated gel values by 3 days (0.52 ± 0.22%). Similar trends were apparent in MDA-MB-231 embedded constructs (Figures 6b and 6d). The F-actin area fraction was 4.1 ± 0.6% at 0 day, 4.5 ± 0.3% at 1 day, and 2.1 ± 0.1% at 3 days in aspirated gels. Unaspirated gels had a lower F-actin area fraction initially at 0.9 ± 0.3% at 0 day, but became similar by 3 days (2.5 ± 0.5%).

3.4 | Gel aspiration affects embedded cancer cell number density in postculture of dermal-punched gels

Gel aspiration affected the number density of embedded cancer cells (Figure 7). The number density of MDA-MB-231 cells (Figure 7a,b) but not MCF-7 cells (Figure 7c,d) was higher following aspiration than unaspirated controls (Figure 7d,e). Cell number density was higher in aspirated gels than unaspirated gels for MDA-MB-231 cells at all three time points (Figure 7c). The cell density was 63 ± 8, 61 ± 10, and 50 ± 6 cells/mm^2 at 0, 1, and 3 days after aspiration, respectively. Cell density was only lower at 3 days versus 1 day. In unaspirated constructs, cell number density remained lower at 28 ± 5, 33 ± 5 and 36 ± 4 at 0, 1, and 3 days, respectively. MCF-7 cells in aspirated gels were at 35 ± 10, 24 ± 9, and 20 ± 6 cells/mm^2 at 0, 1, and 3 days, respectively, with each cell density at each time point significantly lower than the previous. In unaspirated gels, the density was 22 ± 3, 31 ± 11, and 18 ± 5 cells/mm^2 at 0, 1, and 3 days, respectively, with no significant difference in cell density.

3.5 | Cancer cells proliferated in aspirated gels created from a PDMS mold

Gel aspiration did not prevent cancer cells from proliferating during 3 days culture following the event (Figure 8), dependent on aspiration, culture time, and cell type (F = 14–105, p < .001). At Day 0, immediately following a high-pressure GAE, aspirated gels were 102% and 97% of the unaspirated constructs, for MDA-MB-231 and MCF-7 cells, respectively. By 1 and 3 days after aspiration, both cell types had proliferated, 1.5- and 2-fold higher than baseline at Day 0, but still 78% and 77% of unaspirated control gels' (Figure 8). Differences by posthoc Tukey's test in Figure 8 are indicated by a letter and refer to the group bar below each letter in comparison to the unlabeled bar in the time series of bars (letters *a*–*h*, p < .05). The letter *g* refers to differences between unaspirated versus aspirated groups of the same cell type, across timepoints (p < .01).

Gel construct wet weight and projected area were altered during the culture of the constructs made in the PDMS mold (Table 1). Both gel volume and wet weight were 1.9-fold less in aspirated versus unaspirated gels at Day 0, while cell density was twofold higher in aspirated than unaspirated gels at Day 0, counted from histology sections (Figures 7c and 7e).

4 | DISCUSSION

Breast cancer cells embedded in three-dimensional collagen hydrogels survive high-pressure aspiration-ejection with only transient deformation of the F-actin cytoskeleton, primarily in collagen-adherent MDA-MB-231 cells. High-pressure aspiration elongates and shears gel constructs, producing an aligned, dense collagen network. In contrast, low-pressure

aspiration produces a less uniform gel deformation, with a compacted front edge, shear at the gel sides, and folding of the trailing edge (Figures 2 and S3). Aspiration-ejection created compact, pill-shaped gel constructs, leading to an immediately higher number density of embedded cancer cells, many of which coaligned with an anisotropic collagen network in the direction of aspiration (Figure 4). Still, viable, adherent cancer cells remained in culture 3 days after aspiration despite the seeming large stresses imposed on the collagen network and cells. These data suggest the long-term viability of cancer cells in dense, aligned collagen gels created by aspiration-ejection. Proliferation of both cell types occurred when the constructs were gently extruded from a PDMS mold (Figures 8 and S2), rather than from constructs created using a dermal punch, which produced stable or slightly decreasing cell counts (Figure 7). Taken together, these data suggest gel aspiration produces an immediate, purely physical remodeling effect by applying stress to the deformed gel and embedded cells, which continue to proliferate and remodel the collagen network in subsequent culture.

The strengths and weaknesses of the present study derive from the methods used and the study design. High collagen density and alignment of aspirated gels mimics the in vivo ECM microstructure of some tumors, which influences cancer disease features (Barcus, Holt, Keely, Eliceiri, & Schuler, 2015; Brisson et al., 2015; Riching et al., 2014). To characterize this novel biofabrication approach for cancer cell constructs, gels were subjected to two different aspiration pressures (Figure S3), and embedded with two breast cancer cell lines, to gauge potential effects of the aspiration protocol and cell type on cancer cell proliferation in culture and behavior at postaspiration timepoints. The trends in measurements from these cell lines and timepoints confirm that viable cells remain embedded in the dense, aligned collagen network for up to 72 hr of subsequent culture, while pointing to several key differences. For example, embedded MDA-MB-231 were more elongated than MCF-7 cells, which produced an immediate alignment of individual MDA-MB-231 cells (Figure 5, Day 0) versus aligned clusters of MCF-7 cells (Figure 5, Day 0). This alignment of elongated individual cells and clusters can be interpreted in light of the well-known greater cell–cell connections of MCF-7 cells than MDA-MB-231 (Kudo et al., 2009), but also in the postulated property of collagen hydrogels to deform under mechanical stress while cushioning embedded cells that experience only a fraction of that total stress, modulated by cell stiffness (Gyoneva et al., 2016). A weakness of the study was the use of a dermal punch to create the tissue constructs, which appears to have damaged some cells, leading to lower F-actin area fraction (Figure 6) and cell number density in the histology section (Figure 7) over culture time. To address this, we conducted an additional experiment using a PDMS gel mold that reliably creates collagen gels for aspiration, in which the gels can be released into floating culture by the gentle flow of media from a micropipette, avoiding mixing issues in a Petri dish that could make cell counts locally off (see Figures 8 and S2, Table 1). This method is likely gentler than using a dermal punch to create constructs, so the loss of wet weight and projected area, the latter only significant for unaspirated gels at Day 3, is telling of some level of active remodeling of the collagen network by metabolically active cells. The initial twofold difference in these volume-approximating measurements from aspirated and unaspirated constructs corresponds to the two times increase in cell number density in histology sections at Day 0 (Figure 7). After that, while some remodeling is apparent in confocal micrographs of aspirated gels, especially by Day 3 (Figure 5a),

most bulk alterations occur in unaspirated gels (Table 1). indicating reasonable stability of the compact, aligned constructs. Many cancer cells persisted in the gels over 3 days of subsequent culture (Figures 4-6). Future studies will attempt greater control of domains of microstructure within the aspirated gel (e.g., see Figure S4) by varying the magnitude of pressure steps during low-pressure aspiration and will test the constructs mechanically, for example with nanoindentation (Kaufman & Klapperich, 2009). The high-pressure aspiration produced a higher aspect ratio construct (Figure S3), but possibly also applied higher stress to embedded cells, although cells were still able to proliferate in these constructs (Figure 8).

This study demonstrates that GAE has minimal damaging effects on embedded cancer cells, supporting subsequent culture in aligned, dense collagen constructs. As such, the present study introduces a tissue culture platform that supports recent efforts to create aligned, denser models of tumor stroma (Rubiano et al., 2018), to better understand how such properties regulate cancer behavior, promoting survival and progression (Case et al., 2017; Cheon et al., 2014; Gruionu et al., 2016; Hong, Kim, Li, Jeong, & Yoon, 2017; Pointer et al., 2017). Future work will determine whether cancer cell-embedded, aspirated gels can feasibly be implanted into mouse models to study the effect of novel therapeutic agents or ECM-dependent cancer behavior in a preclinical, in vivo setting. Toward this aim, longer culture (>3 days) postaspiration is needed to evaluate whether the surviving cancer cells are able to invade through the constructs and into adjacent tissue regions. In contrast, the present study sought to determine the feasibility of the aspiration approach to create dense, aligned constructs with viable cancer cells. In the tumor, tensile forces are likely derived from contractility of tumor-associated fibroblasts (Garcia-Palmero et al., 2016), and remodeling activity of the cancer cells themselves (Hwang, Oh, Lee, & Kuh, 2019). Alignment of dense collagen in the stroma may also result from compressive stress from the growing tumor (Chauhan et al., 2014; Cheng, Tse, Jain, & Munn, 2009), or may already exist, for example, in the metastatic niche. Collagen GAE creates dense, aligned in vitro tissue constructs in which cancer cell location and morphology can be tracked during culture, and multiple assessments made to discern cancer responses to local microenvironments. The current study demonstrates the feasibility of this platform, allowing its future use to determine interactions of cancer cells with their microstructural microenvironment. Cell migration through dense, aligned microenvironments is of particular interest (Wolf et al., 2013) as this may be modulated by multiscale mechanics (Taufalele, VanderBurgh, Munoz, Zanotelli, & Reinhart-King, 2019) and quite a difficult task for cells in terms of energy expenditure (Zanotelli et al., 2018), yet is clearly important to wound healing (Dubois, Kalashnikov, & Moraes, 2019), cancer metastasis (Ferruzzi, Zhang, Roblyer, & Zaman, 2020; Wirtz, Konstantopoulos, & Searson, 2011), and other (patho)physiological processes (Bonnans, Chou, & Werb, 2014).

The parallel orientation of individual cells and cell clusters with collagen microstructural alignment indicates the role of passive cell and collagen network mechanics in determining the initial response to aspiration stresses. Two pieces of evidence suggest the alignment effect stemmed directly from applied forces, rather than exclusively contact guidance of cells by the collagen network. First, gels fixed immediately after aspiration contained aligned cells and clusters (Figures 4 and 5, Day 0). Occasionally, MDA-MB-231 cells appeared warped into the alignment direction, as in the first panel of Figure 5a, which

could be an effect of the relative compliance of these cells (Rudzka et al., 2019). It would be interesting to test whether the ability of MDA-MB-231 cells to align with a collagen network depends on the amount of applied mechanical stress, collagen network density and topology, or focal adhesions.

In conclusion, aspiration-ejection rapidly assembles three-dimensional models of the dense, aligned collagen network microstructure within the tumor stroma and local microenvironment. Breast cancer prognosis is related to tissue-level collagen alterations in animal models and humans. Therefore, the findings of the present study represent an important step toward biofabrication of more clinically relevant in vitro models of breast cancer. In the future, GAE may serve as a platform to study specific interactions of cancer cells with ECM, including matrix invasion, tumor cell proliferation, and response to chemotherapies. Parallelization and automation of aspiration-ejection could allow the technique to be used in the future to biofabricate tumor tissue models for high throughput drug screening. A manifold aspiration system aligned to a 96- or 386-wellplates format could facilitate this development.

Supplementary Material

Refer to Web version on PubMed Central for supplementary material.

ACKNOWLEDGMENTS

The authors acknowledge funding support from the National Institute of Diabetes and Digestive and Kidney Diseases (DK102043) to C. B. R. and B. C. B. and National Institute of Biomedical Imaging and Bioengineering (EB021483) to X. L. and B. C. B., and separately (EB028017) to C. B. R. as well as the CUA School of Engineering and the New Millennium Scholarship for R. H.

REFERENCES

Barcus CE, Holt EC, Keely PJ, Eliceiri KW, & Schuler LA (2015). Dense collagen-I matrices enhance pro-tumorigenic estrogen-prolactin crosstalk in MCF-7 and T47D breast cancer cells. PLOS One, 10(1):e0116891. 10.1371/journal.pone.0116891 [PubMed: 25607819]

Bessea L, Coulomb B, Lebreton-Decoster C, & Giraud-Guille MM (2002). Production of ordered collagen matrices for three-dimensional cell culture. Biomaterials, 23(1), 27–36. [PubMed: 11762846]

Bonnans C, Chou J, & Werb Z (2014). Remodelling the extracellular matrix in development and disease. Nature Reviews Molecular Cell Biology, 15(12), 786–801. 10.1038/nrm3904 [PubMed: 25415508]

Bordeleau F, Mason BN, Lollis EM, Mazzola M, Zanotelli MR, Somasegar S, … Reinhart-King CA (2017). Matrix stiffening promotes a tumor vasculature phenotype. Proceedings of the National Academy of Sciences of the United States of America, 114(3), 492–497. 10.1073/pnas.1613855114 [PubMed: 28034921]

Boyd NF, Martin LJ, Stone J, Greenberg C, Minkin S, & Yaffe MJ (2001). Mammographic densities as a marker of human breast cancer risk and their use in chemoprevention. Current Oncology Reports, 3(4), 314–321. [PubMed: 11389815]

Brabek J, Mierke CT, Rosel D, Vesely P, & Fabry B (2010). The role of the tissue microenvironment in the regulation of cancer cell motility and invasion. Cell Communication and Signaling, 8, 22. 10.1186/1478-811X-8-22 [PubMed: 20822526]

Brisson BK, Mauldin EA, Lei W, Vogel LK, Power AM, Lo A, … Volk SW (2015). Type III collagen directs stromal organization and limits metastasis in a murine model of breast cancer. American Journal of Pathology, 185(5), 1471–1486. 10.1016/j.ajpath.2015.01.029

Brown R, Wiseman M, Chuo C, Cheema U, & Nazhat S (2005). Ultrarapid engineering of biomimetic materials and tissues: Fabrication of nano- and microstructures by plastic compression. Advanced Functional Materials, 15, 1762–1770. 10.1002/adfm.200500042

Case A, Brisson BK, Durham AC, Rosen S, Monslow J, Buza E, … Volk SW (2017). Identification of prognostic collagen signatures and potential therapeutic stromal targets in canine mammary gland carcinoma. PLOS One, 12(7):e0180448. 10.1371/journal.pone.0180448 [PubMed: 28683102]

Chauhan VP, Boucher Y, Ferrone CR, Roberge S, Martin JD, Stylianopoulos T, … Jain RK (2014). Compression of pancreatic tumor blood vessels by hyaluronan is caused by solid stress and not interstitial fluid pressure. Cancer Cell, 26(1), 14–15. 10.1016/j.ccr.2014.06.003 [PubMed: 25026209]

Cheng G, Tse J, Jain RK, & Munn LL (2009). Micro-environmental mechanical stress controls tumor spheroid size and morphology by suppressing proliferation and inducing apoptosis in cancer cells. PLOS One, 4(2):e4632. 10.1371/journal.pone.0004632 [PubMed: 19247489]

Cheon DJ, Tong Y, Sim MS, Dering J, Berel D, Cui X, … Orsulic S (2014). A collagen-remodeling gene signature regulated by TGF-beta signaling is associated with metastasis and poor survival in serous ovarian cancer. Clinical Cancer Research, 20(3), 711–723. 10.1158/1078-0432.CCR-13-1256 [PubMed: 24218511]

Conklin MW, Eickhoff JC, Riching KM, Pehlke CA, Eliceiri KW, Provenzano PP, … Keely PJ (2011). Aligned collagen is a prognostic signature for survival in human breast carcinoma. American Journal of Pathology, 178(3), 1221–1232. 10.1016/j.ajpath.2010.11.076

Dong Y, Xie X, Wang Z, Hu C, Zheng Q, Wang Y, … Cui J (2014). Increasing matrix stiffness upregulates vascular endothelial growth factor expression in hepatocellular carcinoma cells mediated by integrin beta1. Biochemical and Biophysical Research Communications, 444(3), 427–432. 10.1016/j.bbrc.2014.01.079 [PubMed: 24472554]

Dubois SJ, Kalashnikov N, & Moraes C (2019). Robust and precise wounding and analysis of engineered contractile tissues. Tissue Engineering. Part C, Methods, 25(11), 677–686. 10.1089/ten.TEC.2019.0123 [PubMed: 31411125]

Eberl C (2020). Digital Image Correlation and Tracking, MATLAB Central File Exchange. Retrieved from https://www.mathworks.com/matlabcentral/fileexchange/12413-digital-image-correlation-and-tracking

Engler AJ, Sen S, Sweeney HL, & Discher DE (2006). Matrix elasticity directs stem cell lineage specification. Cell, 126(4), 677–689. 10.1016/j.cell.2006.06.044 [PubMed: 16923388]

Esbona K, Yi Y, Saha S, Yu M, Van Doorn RR, Conklin MW, … Keely PJ (2018). The presence of cyclooxygenase 2, tumor-associated macrophages, and collagen alignment as prognostic markers for invasive breast carcinoma patients. American Journal of Pathology, 188(3), 559–573. 10.1016/j.ajpath.2017.10.025

Fang M, Yuan J, Peng C, & Li Y (2014). Collagen as a double-edged sword in tumor progression. Tumour Biology, 35(4), 2871–2882. 10.1007/s13277-013-1511-7 [PubMed: 24338768]

Ferruzzi J, Zhang Y, Roblyer D, & Zaman MH (2020). Multi-scale mechanics of collagen networks: Biomechanical basis of matrix remodeling in cancer. In Zhang Y (Ed.), Multi-scale extracellular matrix mechanics and mechanobiology (pp. 343–387). Cham, Switzerland: Springer International Publishing.

Fonck E, Feigl GG, Fasel J, Sage D, Unser M, Rufenacht DA, & Stergiopulos N (2009). Effect of aging on elastin functionality in human cerebral arteries. Stroke, 40(7), 2552–2556. 10.1161/Strokeaha.108.528091 [PubMed: 19478233]

Garcia-Palmero I, Torres S, Bartolome RA, Pelaez-Garcia A, Larriba MJ, Lopez-Lucendo M, … Casal JI (2016). Twist1-induced activation of human fibroblasts promotes matrix stiffness by upregulating palladin and collagen alpha1(VI). Oncogene, 35(40), 5224–5236. 10.1038/onc.2016.57 [PubMed: 26973246]

Gruionu G, Bazou D, Maimon N, Onita-Lenco M, Gruionu LG, Huang P, & Munn LL (2016). Implantable tissue isolation chambers for analyzing tumor dynamics in vivo. Lab on a Chip, 16(10), 1840–1851. 10.1039/c6lc00237d [PubMed: 27128791]

Guo WH, Frey MT, Burnham NA, & Wang YL (2006). Substrate rigidity regulates the formation and maintenance of tissues. Biophysical Journal, 90(6), 2213–2220. 10.1529/biophysj.105.070144 [PubMed: 16387786]

Gyoneva L, Hovell CB, Pewowaruk RJ, Dorfman KD, Segal Y, & Barocas VH (2016). Cell-matrix interaction during strain-dependent remodelling of simulated collagen networks. Interface Focus, 6(1): 20150069. 10.1098/rsfs.2015.0069 [PubMed: 26855754]

Han W, Chen S, Yuan W, Fan Q, Tian J, Wang X, … Liu L (2016). Oriented collagen fibers direct tumor cell intravasation. Proceedings of the National Academy of Sciences of the United States of America, 113(40), 11208–11213. 10.1073/pnas.1610347113 [PubMed: 27663743]

Hong Y, Kim N, Li C, Jeong E, & Yoon S (2017). Patient sample-oriented analysis of gene expression highlights extracellular signatures in breast cancer progression. Biochemical and Biophysical Research Communications, 487(2), 307–312. 10.1016/j.bbrc.2017.04.055 [PubMed: 28412350]

Hwang HJ, Oh MS, Lee DW, Kuh HJ (2019). Multiplex quantitative analysis of stroma-mediated cancer cell invasion, matrix remodeling, and drug response in a 3D co-culture model of pancreatic tumor spheroids and stellate cells. Journal of Experimental & Clinical Cancer Research, 38(1), 258. 10.1186/s13046-019-1225-9 [PubMed: 31200779]

Jones EMC, Silberstein MN, White SR, & Sottos NR (2014). In situ measurements of strains in composite battery electrodes during electrochemical cycling. Experimental Mechanics, 54(6), 971–985. 10.1007/s11340-014-9873-3

Kamranpour NO, Miri AK, James-Bhasin M, & Nazhat SN (2016). A gel aspiration-ejection system for the controlled production and delivery of injectable dense collagen scaffolds. Biofabrication, 8(1): 015018. 10.1088/1758-5090/8/1/015018 [PubMed: 27003606]

Kaufman JD, & Klapperich CM (2009). Surface detection errors cause overestimation of the modulus in nanoindentation on soft materials. Journal of the Mechanical Behavior of Biomedical Materials, 2(4), 312–317. 10.1016/j.jmbbm.2008.08.004 [PubMed: 19627837]

Keating M, Kurup A, Alvarez-Elizondo M, Levine AJ, & Botvinick E (2017). Spatial distributions of pericellular stiffness in natural extracellular matrices are dependent on cell-mediated proteolysis and contractility. Acta Biomaterialia, 57, 304–312. 10.1016/j.actbio.2017.05.008 [PubMed: 28483696]

Keating M, Lim M, Hu Q, & Botvinick E (2019). Selective stiffening of fibrin hydrogels with micron resolution via photocrosslinking. Acta Biomaterialia, 87, 88–96. 10.1016/j.actbio.2019.01.034 [PubMed: 30660778]

Knight DP, Nash L, Hu XW, Haffegee J, & Ho MW (1998). In vitro formation by reverse dialysis of collagen gels containing highly oriented arrays of fibrils. Journal of Biomedical Materials Research, 41(2), 185–191. [PubMed: 9638522]

Kocsis K, Hyttinen M, Helminen HJ, Aydelotte MB, & Modis L (1998). Combination of digital image analysis and polarization microscopy: Theoretical considerations and experimental data. Microscopy Research and Technique, 43(6), 511–517. 10.1002/(SICI)1097-0029(19981215)43:6<511::AID-JEMT4>3.0.CO;2-A [PubMed: 9880165]

Kudo T, Kigoshi H, Hagiwara T, Takino T, Yamazaki M, & Yui S (2009). Cathepsin G, a neutrophil protease, induces compact cell-cell adhesion in MCF-7 human breast cancer cells. Mediators of Inflammation, 2009, 850940–11. 10.1155/2009/850940 [PubMed: 19920860]

Levental KR, Yu H, Kass L, Lakins JN, Egeblad M, Erler JT, … Weaver VM (2009). Matrix crosslinking forces tumor progression by enhancing integrin signaling. Cell, 139(5), 891–906. 10.1016/j.cell.2009.10.027 [PubMed: 19931152]

Marelli B, Ghezzi CE, James-Bhasin M, & Nazhat SN (2015). Fabrication of injectable, cellular, anisotropic collagen tissue equivalents with modular fibrillar densities. Biomaterials, 37, 183–193. 10.1016/j.biomaterials.2014.10.019 [PubMed: 25453949]

Mi S, Chen B, Wright B, & Connon CJ (2010). Ex vivo construction of an artificial ocular surface by combination of corneal limbal epithelial cells and a compressed collagen scaffold containing

keratocytes. Tissue Engineering. Part A, 16(6), 2091–2100. 10.1089/ten.TEA.2009.0748 [PubMed: 20109018]

Miri AK, Muja N, Kamranpour NO, Lepry WC, Boccaccini AR, Clarke SA, & Nazhat SN (2016). Ectopic bone formation in rapidly fabricated acellular injectable dense collagen-Bioglass hybrid scaffolds via gel aspiration-ejection. Biomaterials, 85, 128–141. 10.1016/j.biomaterials.2016.01.047 [PubMed: 26871889]

Pelham RJ Jr., & Wang Y (1997). Cell locomotion and focal adhesions are regulated by substrate flexibility. Proceedings of the National Academy of Sciences of the United States of America, 94(25), 13661–13665. [PubMed: 9391082]

Pointer KB, Clark PA, Schroeder AB, Salamat MS, Eliceiri KW, & Kuo JS (2017). Association of collagen architecture with glioblastoma patient survival. Journal of Neurosurgery, 126(6), 1812–1821. 10.3171/2016.6.JNS152797 [PubMed: 27588592]

Provenzano PP, Eliceiri KW, Campbell JM, Inman DR, White JG, & Keely PJ (2006). Collagen reorganization at the tumor-stromal interface facilitates local invasion. BMC Medicine, 4(1), 38. 10.1186/1741-7015-4-38 [PubMed: 17190588]

Raeber GP, Lutolf MP, & Hubbell JA (2005). Molecularly engineered PEG hydrogels: A novel model system for proteolytically mediated cell migration. Biophysical Journal, 89(2), 1374–1388. 10.1529/biophysj.104.050682 [PubMed: 15923238]

Raub CB, Hsu SC, Chan EF, Shirazi R, Chen AC, Chnari E, … Sah RL (2013). Microstructural remodeling of articular cartilage following defect repair by osteochondral autograft transfer. Osteoarthritis and Cartilage, 21(6), 860–868. 10.1016/j.joca.2013.03.014 [PubMed: 23528954]

Raub CB, Suresh V, Krasieva T, Lyubovitsky J, Mih JD, Putnam AJ, … George SC (2007). Noninvasive assessment of collagen gel microstructure and mechanics using multiphoton microscopy. Biophysical Journal, 92(6), 2212–2222. 10.1529/biophysj.106.097998 [PubMed: 17172303]

Reinhart-King CA, Dembo M, & Hammer DA (2008). Cell-cell mechanical communication through compliant substrates. Biophysical Journal, 95(12), 6044–6051. 10.1529/biophysj.107.127662 [PubMed: 18775964]

Rezakhaniha R, Agianniotis A, Schrauwen JTC, Griffa A, Sage D, Bouten CVC, … Stergiopulos N (2012). Experimental investigation of collagen waviness and orientation in the arterial adventitia using confocal laser scanning microscopy. Biomechanics and Modeling in Mechanobiology, 11(3-4), 461–473. 10.1007/s10237-011-0325-z [PubMed: 21744269]

Riching KM, Cox BL, Salick MR, Pehlke C, Riching AS, Ponik SM, … Keely PJ (2014). 3D collagen alignment limits protrusions to enhance breast cancer cell persistence. Biophysical Journal, 107(11), 2546–2558. 10.1016/j.bpj.2014.10.035 [PubMed: 25468334]

Rieppo J, Hallikainen J, Jurvelin JS, Kiviranta I, Helminen HJ, & Hyttinen MM (2008). Practical considerations in the use of polarized light microscopy in the analysis of the collagen network in articular cartilage. Microscopy Research and Technique, 71(4), 279–287. 10.1002/jemt.20551 [PubMed: 18072283]

Rubiano A, Delitto D, Han S, Gerber M, Galitz C, Trevino J, … Simmons CS (2018). Viscoelastic properties of human pancreatic tumors and in vitro constructs to mimic mechanical properties. Acta Biomaterialia, 67, 331–340. 10.1016/j.actbio.2017.11.037 [PubMed: 29191507]

Rudzka DA, Spennati G, McGarry DJ, Chim YH, Neilson M, Ptak A, … Olson MF (2019). Migration through physical constraints is enabled by MAPK-induced cell softening via actin cytoskeleton reorganization. Journal of Cell Science, 132(11):jcs224071. 10.1242/jcs.224071 [PubMed: 31152052]

Saeidi N, Guo X, Hutcheon AE, Sander EA, Bale SS, Melotti SA, … Ruberti JW (2012). Disorganized collagen scaffold interferes with fibroblast mediated deposition of organized extracellular matrix in vitro. Biotechnology and Bioengineering, 109(10), 2683–2698. 10.1002/bit.24533 [PubMed: 22528405]

Shebanova O, & Hammer DA (2012). Biochemical and mechanical extracellular matrix properties dictate mammary epithelial cell motility and assembly. Biotechnology Journal, 7(3), 397–408. 10.1002/biot.201100188 [PubMed: 22121055]

Shribak M, & Oldenbourg R (2003). Techniques for fast and sensitive measurements of two-dimensional birefringence distributions. Applied Optics, 42(16), 3009–3017. 10.1364/ao.42.003009 [PubMed: 12790452]

Taufalele PV, VanderBurgh JA, Munoz A, Zanotelli MR, & Reinhart-King CA (2019). Fiber alignment drives changes in architectural and mechanical features in collagen matrices. PLOS One, 14(5):e0216537. 10.1371/journal.pone.0216537 [PubMed: 31091287]

Thevenaz P, & Unser M (2007). User-friendly semiautomated assembly of accurate image mosaics in microscopy. Microscopy Research and Technique, 70(2), 135–146. 10.1002/jemt.20393 [PubMed: 17133410]

Thula TT, Rodriguez DE, Lee MH, Pendi L, Podschun J, & Gower LB (2011). In vitro mineralization of dense collagen substrates: A biomimetic approach toward the development of bone-graft materials. Acta Biomaterialia, 7(8), 3158–3169. 10.1016/j.actbio.2011.04.014 [PubMed: 21550424]

Tower TT, & Tranquillo RT (2001). Alignment maps of tissues: II. Fast harmonic analysis for imaging. Biophysical Journal, 81(5), 2964–2971. 10.1016/S0006-3495(01)75936-X [PubMed: 11606306]

Vader D, Kabla A, Weitz D, & Mahadevan L (2009). Strain-induced alignment in collagen gels. PLOS One, 4(6):e5902. 10.1371/journal.pone.0005902 [PubMed: 19529768]

Wei SC, Fattet L, Tsai JH, Guo Y, Pai VH, Majeski HE, … Yang J (2015). Matrix stiffness drives epithelial-mesenchymal transition and tumour metastasis through a TWIST1-G3BP2 mechanotransduction pathway. Nature Cell Biology, 17(5), 678–688. 10.1038/ncb3157 [PubMed: 25893917]

Wirtz D, Konstantopoulos K, & Searson PC (2011). The physics of cancer: The role of physical interactions and mechanical forces in metastasis. Nature Reviews Cancer, 11(7), 512–522. 10.1038/nrc3080 [PubMed: 21701513]

Wolf K, Te Lindert M, Krause M, Alexander S, Te Riet J, Willis AL, … Friedl P (2013). Physical limits of cell migration: Control by ECM space and nuclear deformation and tuning by proteolysis and traction force. Journal of Cell Biology, 201(7), 1069–1084. 10.1083/jcb.201210152

Yeung T, Georges PC, Flanagan LA, Marg B, Ortiz M, Funaki M, … Janmey PA (2005). Effects of substrate stiffness on cell morphology, cytoskeletal structure, and adhesion. Cell Motility and the Cytoskeleton, 60(1), 24–34. 10.1002/cm.20041 [PubMed: 15573414]

Yuan Z, Memarzadeh K, Stephen AS, Allaker RP, Brown RA, & Huang J (2018). Development of a 3D collagen model for the in vitro evaluation of magnetic-assisted osteogenesis. Scientific Reports, 8(1): 16270. 10.1038/s41598-018-33455-2 [PubMed: 30389949]

Zaman MH, Trapani LM, Sieminski AL, Mackellar D, Gong H, Kamm RD, … Matsudaira P (2006). Migration of tumor cells in 3D matrices is governed by matrix stiffness along with cell-matrix adhesion and proteolysis. Proceedings of the National Academy of Sciences of the United States of America, 103(29), 10889–10894. 10.1073/pnas.0604460103 [PubMed: 16832052]

Zanotelli MR, Goldblatt ZE, Miller JP, Bordeleau F, Li J, VanderBurgh JA, … Reinhart-King CA (2018). Regulation of ATP utilization during metastatic cell migration by collagen architecture. Molecular Biology of the Cell, 29(1), 1–9. 10.1091/mbc.E17-01-0041 [PubMed: 29118073]

Zustiak SP, Dadhwal S, Medina C, Steczina S, Chehreghanianzabi Y, Ashraf A, & Asuri P (2016). Three-dimensional matrix stiffness and adhesive ligands affect cancer cell response to toxins. Biotechnology and Bioengineering, 113(2), 443–452. 10.1002/bit.25709 [PubMed: 26184715]

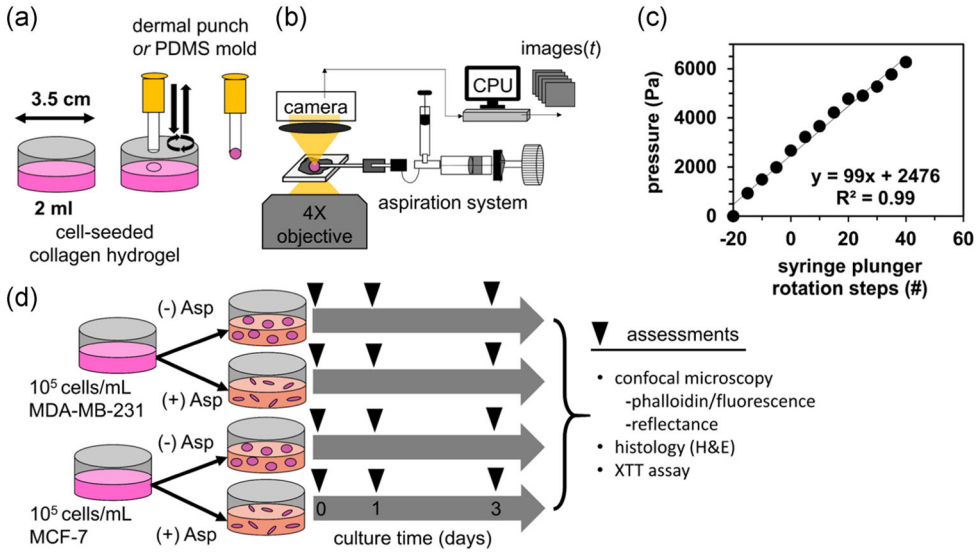

FIGURE 1.

Biofabrication of cancer cell-seeded collagen hydrogel constructs using gel aspiration-ejection. (a) Collagen disks were created using a dermal punch or extruding from a PDMS mold on gels polymerized in Petri dishes. (b) The punched disks were transferred to a gel aspiration system, under an inverted phase-contrast microscope to observe rapid gel deformation. (c) The aspiration pressure was calibrated to the rotation of the knob controlling plunger position of the oil-filled syringe by connecting the capillary tube to a second syringe with a fixed plunger, housing a pressure sensor. (d) Two breast cancer cell lines were cultured in aspirated (+Asp) and unaspirated (−Asp) gels for 3 days, with assessments taken at the indicated timepoints. H&E, hematoxylin and eosin; PDMS, polydimethylsiloxane; XTT, 2,3-Bis(2-methoxy-4-nitro-5-sulfophenyl)-2H-tetrazolium-5-carboxanilide salt

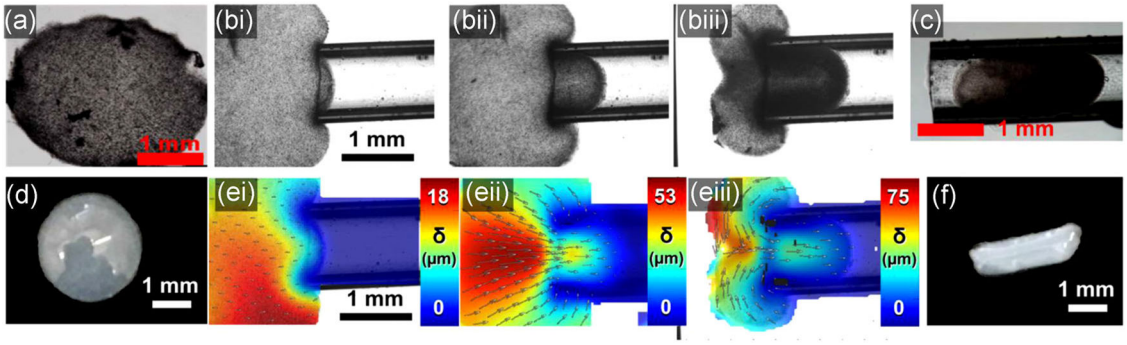

FIGURE 2.

A gel constructs before, during and after aspiration-ejection. Single and mosaiced phase-contrast images of a representative collagen gel (a) before, (bi–iii) during, and (c) after aspiration. (d and f) Profile images of a representative gel disk before aspiration and after subsequent ejection. (ei–iii) Intratissue displacement map overlaid on phase-contrast images at several stages of aspiration. Scale bars are indicated

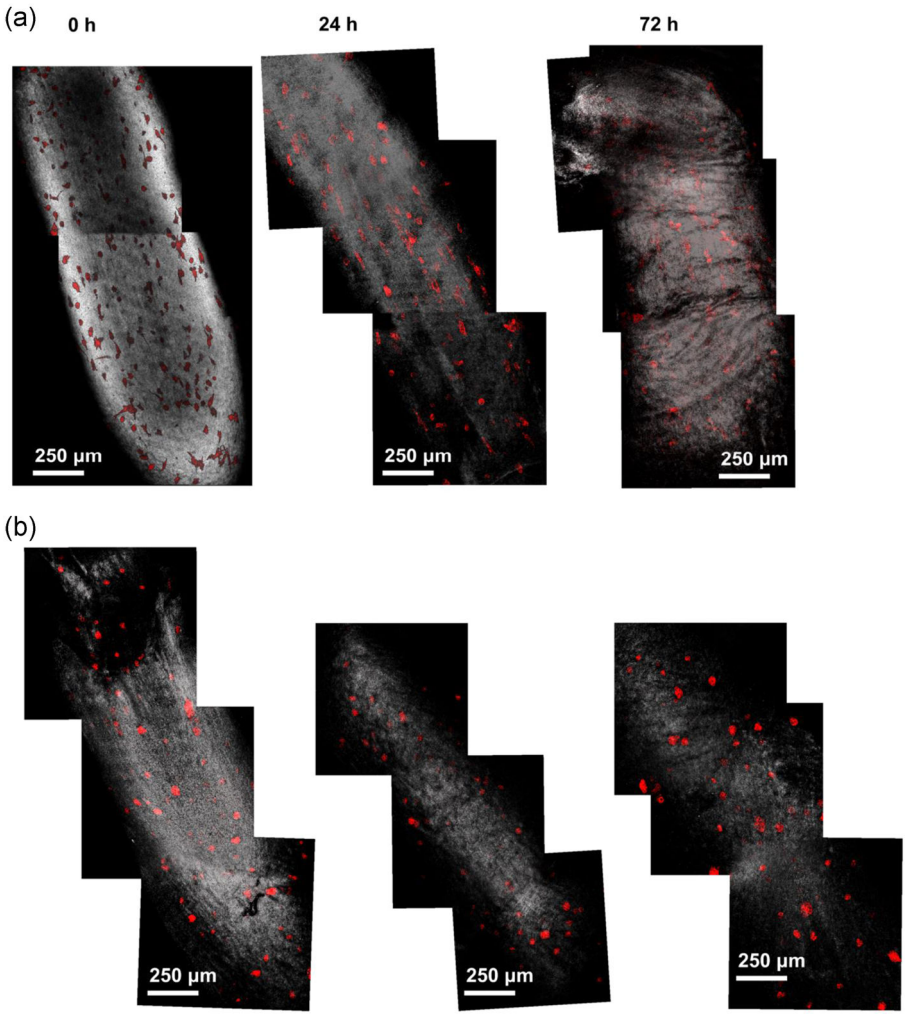

FIGURE 3.

Stitched projections of confocal micrographs of aspirated gels containing embedded (a) MDA-MB-231, and (b) MCF-7 cancer cells, at Day 0, 0 hr (immediately after aspiration-ejection) and after 24 and 72 hr (1 and 3 days, respectively) subsequent culture. The gray signal is reflectance; the red signal is the fluorescence of a phalloidin conjugate. Scale bars are indicated

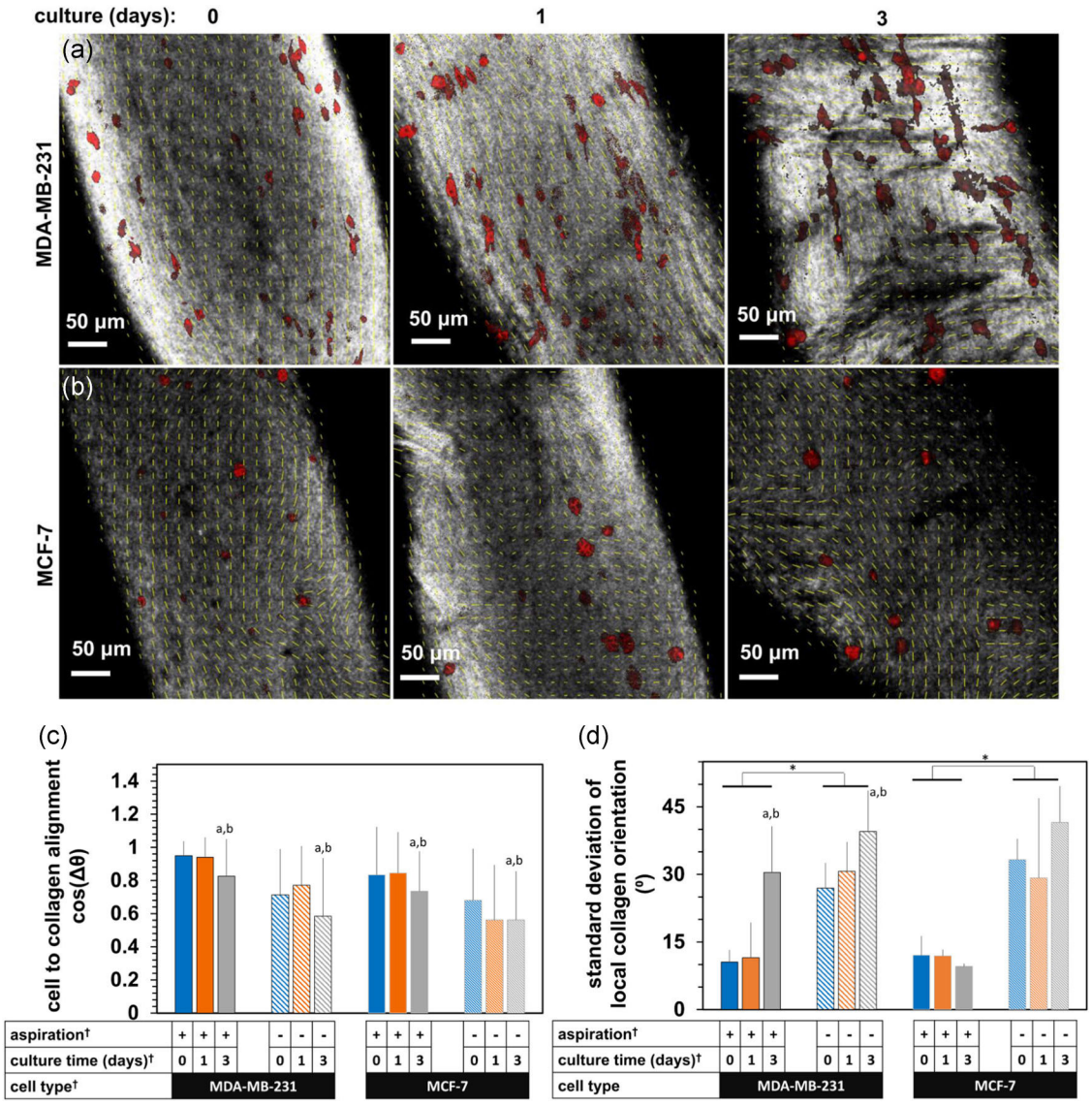

FIGURE 4.

The effects of aspiration-ejection on the collagen microstructure and cell alignment. Confocal micrographs of F-actin signal (red) and reflectance signal primarily from collagen (gray) in (a) MDA-MB-231 and (b) MCF-7 cells within gels with ([+] Asp) and without ([−] Asp) aspiration-ejection, at 0, 1, and 3 days after aspiration. Scale bars are indicated. (c) The average cosine difference angle between local collagen and cell alignment directions, and (d) the standard deviation of local collagen orientations calculated over a scale of 20 pixels/5.3 μm. The † indicator shows significant effects by analysis of variance, $p < .001$. The [a], [b], and * indicators express pairwise differences by Tukey's tests, further indicated by the unlabeled Day 0 for [a] and Day 1 for [b], respectively. Yellow vectors are overlaid local collagen orientation

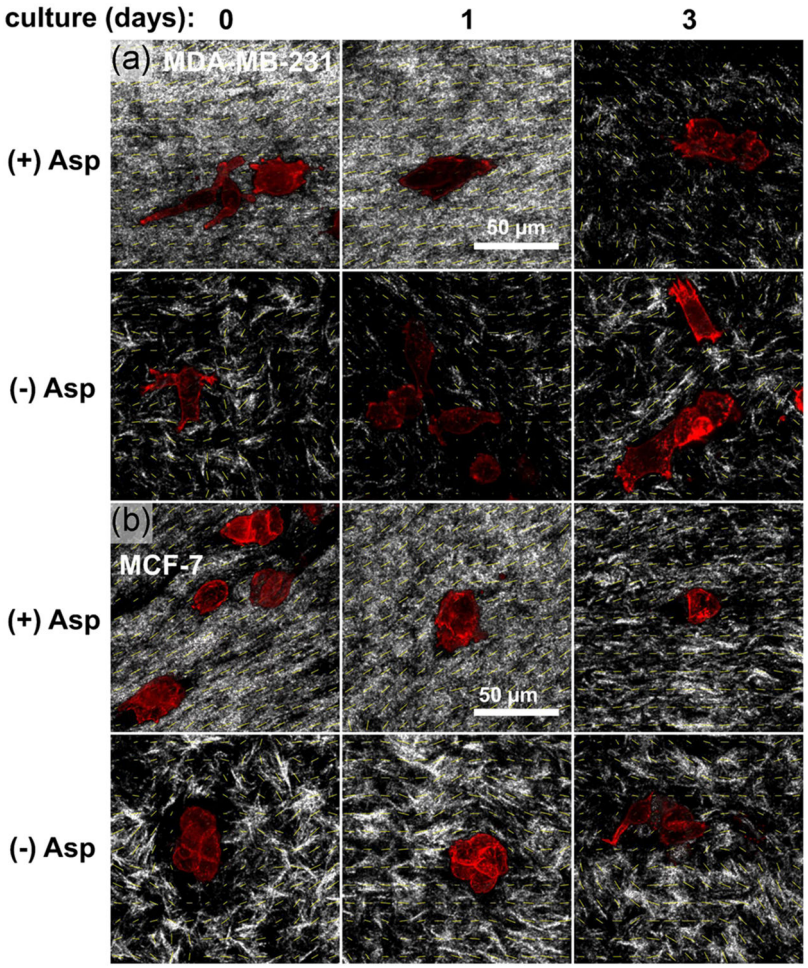

FIGURE 5.

Zoomed-in high-resolution images of interactions between cells and collagen network in aspirated, (+) Asp, and unaspirated, (−) Asp, gels at 0, 1, and 3 days after aspiration of subsequent culture. Red signal is F-actin phalloidin, gray signal is confocal reflectance, and yellow vectors are overlaid local collagen orientation. Scale bars are indicated

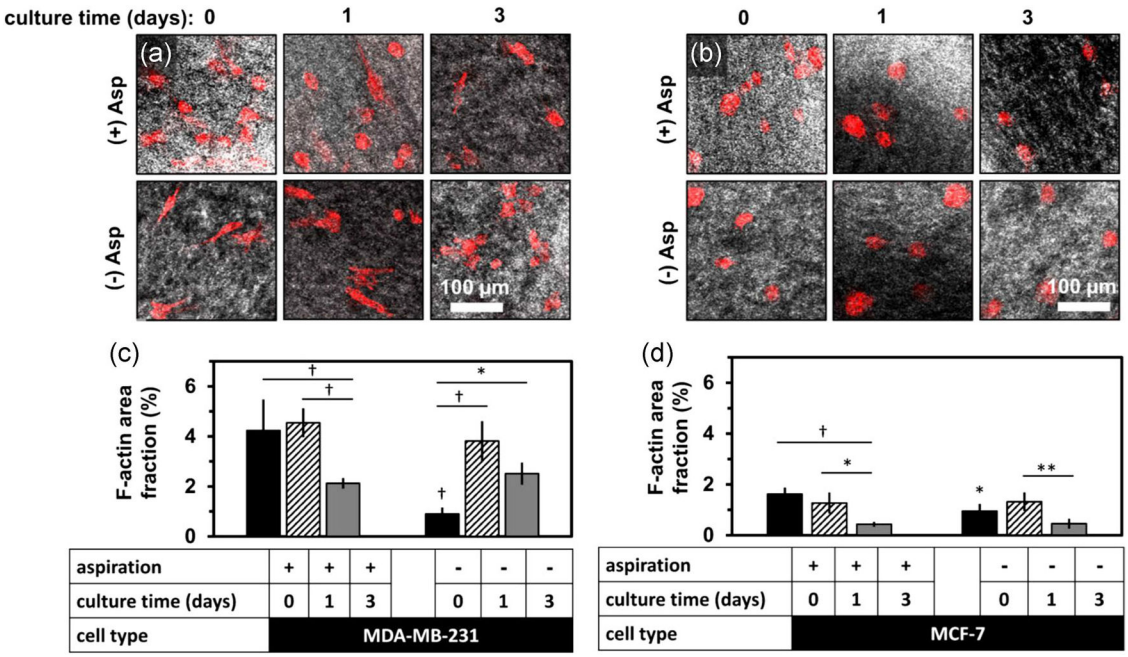

FIGURE 6.

F-actin signal distribution in dermal-punched, aspirated gels versus culture time. F-actin area fraction is higher initially following gel aspiration, then lower by 72 hr. Representative confocal micrographs of confocal reflectance (gray) and F-actin (red) signal of (a) MDA-MB-231 cells and (b) MCF-7 cells after (top row) or without (2nd row) aspiration for 0, 1, and of subsequent culture. The bar graphs show the F-actin staining area fraction per gel for (c) MCF-7 and (d) MDA-MB-231 cells. Data were mean ± standard deviation for a total number of five gels per group. The differences in area fraction due to aspiration and culture time were tested by analysis of variance and posthoc Tukey tests, and were statistically significant: *, **, and † represent $p < .05$, $p < .01$, and $p < .001$, respectively. Markers above horizontal bars connect indicate statistically significant comparisons. Indicators without bars are statistically different from the same culture timepoint, aspiration group

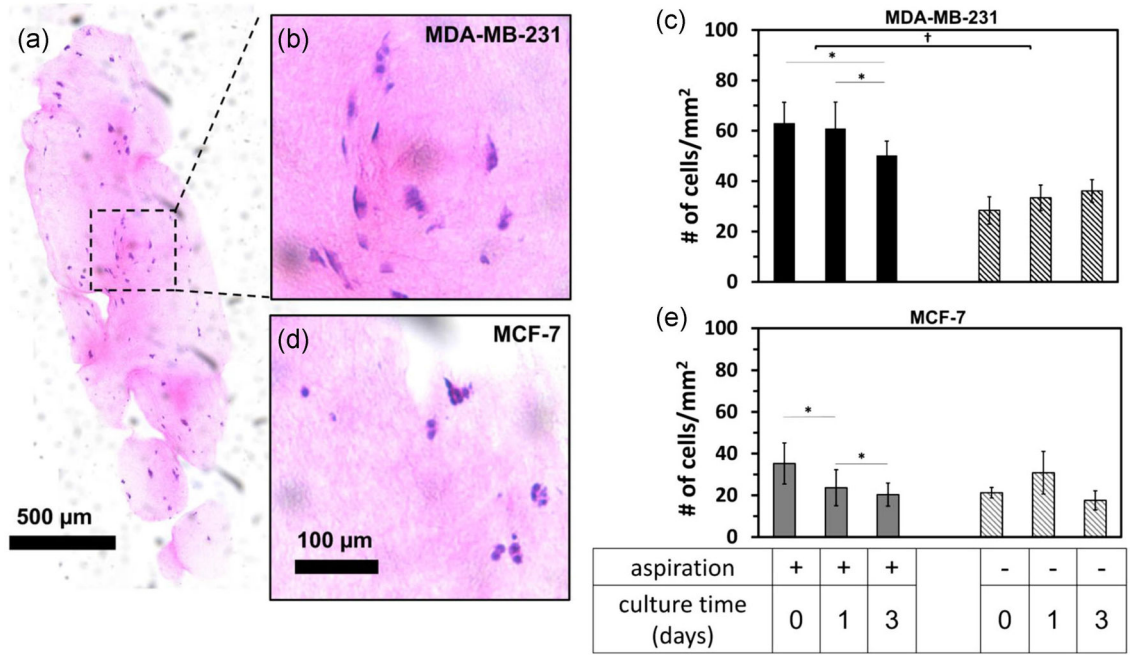

FIGURE 7.

Cell density is affected by aspiration. (a) Hematoxylin and eosin-stained 8 μm-thick mosaiced histology sections of cancer cell-seeded collagen gels following gel aspiration-ejection. Zoom-in sections of (b) MDA-MB-231 and (d) MCF-7 aspirated gels. (c and e) Bar graphs represent cell number density at 0, 1, and 3 days after aspiration-ejection (or paired unaspirated controls). Data were mean ± standard deviation for a total number of five gels per group. The effects of aspiration and culture time were tested by analysis of variance and posthoc Tukey tests for both cell lines and were statistically significant for MDA-MB-231 cell lines: *, **, and † represent $p < .05$, $p < .01$, and $p < .001$, respectively. Markers above horizontal bars connect indicate statistically significant comparisons. Nonparametric the Kruskal–Wallis test was performed for MCF-7 and was significant for culture time but not for aspiration

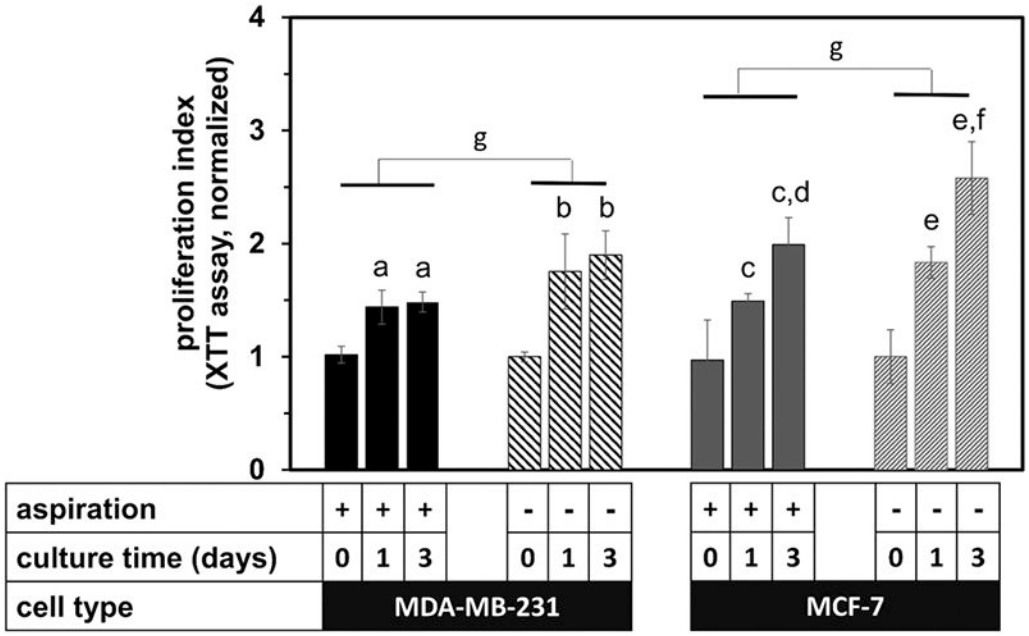

FIGURE 8.

XTT dye absorbance measured from MDA-MB-231 and MCF-7 cell-embedded aspirated gels (+) Asp, and unaspirated controls (−) Asp, at 0, 1, and 3 days after aspiration culture. Data were mean ± *SD* for a total number of five gels per group. XTT signal was normalized to the unaspirated gel at 0 hr as a baseline. Letters indicate $p < .05$ with respect to the corresponding treatment and cell type-matched baseline by Tukey's test. *SD*, standard deviation; XTT, 2,3-Bis(2-methoxy-4-nitro-5-sulfophenyl)-2H-tetrazolium-5-carboxanilide salt

TABLE 1

Physical characteristics of cultured cancer cell-seeded collagen gels following aspiration-ejection

Wet weight (mg, μ ± *SD*)					**Projected area (mm^2, μ ± *SD*)**				
	MDA-MB-231		**MCF-7**			**MDA-MB-231**		**MCF-7**	
Culture (days)*	**(+) Asp****	**(−) Asp****	**(+) Asp****	**(−) Asp****	**Culture (days)†**	**(+) Asp****	**(−) Asp****	**(+) Asp****	**(−) Asp****
0	2.0 ± 0.3	5.8 ± 1.5	3.8 ± 0.8	5.3 ± 1.6	0	3.1 ± 1.0	6.1 ± 1.0	3.6 ± 1.2	6.5 ± 1.3
1	2.0 ± 0.6	6.8 ± 1.3	1.8 ± 0.5	6.1 ± 1.4	1	3.4 ± 1.0	6.2 ± 1.3	3.6 ± 1.3	6.3 ± 1.6
3	2.5 ± 0.9	4.9 ± 1.4	2.0 ± 0.6^{a}	4.0 ± 1.1	3	2.7 ± 1.2	4.0 ± 1.4^{a}	2.2 ± 0.6	4.1 ± 0.8^{a}

Note: Superscripts indicate a significant effect of the independent variable on the dependent (wet weight or projected area) by three-factor ANOVA. Abbreviations: ANOVA, analysis of variance; *SD*, standard deviation.

^{a}Significance between Day 1 and Day 3 group values, by Student's *t*-test, $p < .05$. n = 3–6 gels/group.

* $p < .05$.

** $p < .001$.